Int J Adv Manuf Technol (2017) 93:2655–2666
DOI 10.1007/s00170-017-0469-9

ORIGINAL ARTICLE

Development of a generalized cutting force prediction model for carbon fiber reinforced polymers based on rotary ultrasonic face milling

Muhammad Amin[1,2] · **Songmei Yuan**[1] · **Muhammad Zubair Khan**[2] · **Qi Wu**[1] · **Guangyuan Zhu**[1]

Received: 2 December 2016 / Accepted: 27 April 2017 / Published online: 6 July 2017

Abstract Carbon fiber reinforced polymers (CFRP) have got paramount importance in aircraft, aerospace, and other fields due to their attractive properties of high specific strength/stiffness, high corrosion resistance, and low thermal expansion. These materials have also the properties of inhomogeneity, heterogeneity, anisotropy, and low heat dissipation which generate the issues of excessive cutting forces and machining damages (delamination, fiber pull out, matrix burning, etc.). The cutting forces are required to be modeled for their control/minimization. In this research, a generalized cutting force model has been developed for rotary ultrasonic face milling of CFRP composites. The experimental machining was carried out on CFRP-T700 material. The cutting forces found decreased significantly with the increase of spindle speed while the same found increased with the increase of feed rate and cutting depth. The variation less than 10% has been found between experimental and simulated values (from the model) of cutting forces. However, the higher variation has also observed in the few groups of experiments due to the properties of inhomogeneity, heterogeneity, anisotropy, and low heat dissipation of such materials. The expression for the contact area of the abrasive core tools has been improved and an overlapping cutting allowance has been incorporated the first time. The developed cutting force model has been validated and found robust. So, the generalized cutting force model developed in this paper can be applied to control/minimize the cutting forces for rotary ultrasonic face milling of CFRP composite materials and optimization of the process.

Keywords Rotary ultrasonic face milling · Carbon fiber reinforced polymers · CFRP-T700 · Cutting force · Brittle fracture · Machining parameters

1 Introduction and literature review

Carbon fiber reinforced polymer composites have been widely used in aerospace, automobile, sports, and high-performance supporting equipment, owing to their attractive properties of high specific strength, high specific stiffness, high corrosion resistance, low weight, and low thermal expansion [1, 2]. Particularly, in the aircraft industry, the application of such materials has reached up to 50% by weight (Air bus A-380 of 45%, A350XWB 22%, and Dreamliner 787 by 50% by weight). CFRP is the primary structural material for aircraft and used for panels, stringers/frames of the fuselage to achieve strength/fatigue, and fuel economy by reducing weight [3]. There is an ample need of accurate and damage free machining of such materials as per aerospace standard requirements. However, the issues in machining like excessive cutting forces, higher surface roughness, and damages like delamination, fiber pull-out, fraying, and matrix burning are encountered mainly due to their properties of inhomogeneity, anisotropy, heterogeneity, and low heat dissipation [1, 2]. Also, the cutting phenomenon is complex and required to investigate for accurate machining of such materials. The excessive

Electronic supplementary material The online version of this article (doi:10.1007/s00170-017-0469-9) contains supplementary material, which is available to authorized users.

✉ Songmei Yuan
yuansm@buaa.edu.cn

[1] School of Mechanical Engineering and Automation, Beihang University, Beijing Engineering Technological Research Center of High-efficient and Green CNC Machining Process and Equipment, Beijing 100191, China

[2] Department of Mechanical Engineering, Institute of Space Technology, Islamabad, Pakistan

cutting forces are required to be controlled/minimized through modeling in order to achieve batter surface finish with reduced damages of the machined components. Even these materials are tried to design/manufacture near-to-net shapes, however, some machining processes including drilling and milling are unavoidable. The face milling is also one of the main processes required for precise and accurate dimensions for the components of such materials.

In the last two decades, various machining technologies for brittle materials were developed like cutting, grinding, drilling, and milling [4–7]. However, the machining of newly developed materials was found difficult through conventional methods [8]. In addition, some nontraditional machining processes have also developed such as abrasive water jet machining, electrolytic grinding, electric discharge machining, ultrasonic vibration assisted machining, and rotary ultrasonic machining (RUM) which are applied successfully for machining of brittle materials [9–15].

Rotary ultrasonic machining is a nontraditional machining process which combines the material removal mechanism of diamond grinding and ultrasonic machining. Since its birth in the 1960s, this process has applied in machining of brittle materials like glass, engineering ceramics, silicon, and ceramic matrix composites. In RUM process, a metal-bonded diamond abrasive core tool is ultrasonically vibrated in an axial direction and feeds towards the workpiece at constant feed rate. The motion of the diamond abrasives is the combination of the rotational motion of the spindle, ultrasonic vibration, and feed of the diamond tool. The machining process becomes milling as the feed direction of the tool becomes perpendicular to the direction of ultrasonic vibration and it becomes drilling as the feed direction of the tool becomes parallel to the direction of ultrasonic vibration [16, 17].

The existing literature has revealed that RUM has many advantages over traditional machining, such as lower cutting forces, smaller chipping size, less surface/subsurface damage, and less tool wear [18, 19]. The cutting force is the main characteristic of the machining process and directly affects tool wear, cutting temperature, residual stresses, and surface integrity. The experimental and theoretical research investigations for RUM are available in reasonable numbers. However, the few are related to the modeling of RUM, namely material removal rate, tool wear, and rotary ultrasonic drilling. The rotary ultrasonic face machining was applied the first time and the cutting forces found reduced near to zero after a certain period of time [20]. Further, the conical diamond core tool was applied for rotary ultrasonic face machining and found that cutting depth and feed rate have a significant effect on MRR [21]. The theoretical model for the rotary ultrasonic face milling was developed with the assumption of spherical diamond grit [22]. Yuan et al. proposed a cutting force model for rotary ultrasonic machining of C/SiC composites in ductile mode [23]. The rotary ultrasonic face milling of K9 optical material was carried out with cylindrical diamond core tool, and a mathematical cutting force model was developed [24]. The rotary ultrasonic face milling with conical core tool was carried out, and a cutting force prediction model for ceramic materials was developed [25].

From the literature review, many experimental and theoretical research reports have been found for RUM, but the few of these are related to modeling of cutting forces, material removal rate, and tool wear. Also, the developed cutting force models are mainly related to the rotary ultrasonic drilling process. However, hardly few research reports have been found for rotary ultrasonic face milling (RUFM) of ceramics and other composite materials. The cutting phenomenon for RUFM is still required to be investigated. Also, the research of rotary ultrasonic face milling for CFRP materials has not reported yet. So, keeping in view the rapid increase of wide range applications and the attractive properties, there is an essential need of modeling the cutting forces and related investigations of RUFM for such materials. The excessive cutting forces have adverse effects on properties of composite materials and are required to be modeled for controlling these up to acceptable limits.

In this paper, the mechanistic-based model is developed to predict the cutting forces for RUFM of CFRP composites based on brittle fracture material removal mechanism. The developed model is generalized and is applicable for cylindrical as well as a conical diamond abrasive core tool for the first time. The proportionality parameters (K_1 and K_2) are obtained through designed experiments, calculations, and experimental RUFM of CFRP material with cylindrical and conical abrasive core tools. The developed cutting force model is validated through pilot experiments. The relationship of machining parameters with cutting force is also investigated. Conclusions are drawn in the final section.

2 Development of cutting force model

In this research, rotary ultrasonic face milling has been applied as the combination of ultrasonic vibration process, grinding and milling process, particularly when the ultrasonic vibration direction is perpendicular to the feed direction. The material removal mechanism is based on indentation fracture theory. The cutting process is like a hammer with high frequency mainly effect on the surface of the material discontinuously.

2.1 Establishment of cutting force model

The cutting force model has developed by considering single abrasive grit and then applied summation for all the active abrasive grits. When a diamond abrasive grit penetrates into the surface of the workpiece material, there is a plastic deformation. With the increase of penetration depth, the median

cracks and the lateral cracks grow/generate as shown in Fig. 1. The extended lateral cracks then induce and peeling off the workpiece material. The maximum penetration depth has been used as an intermediate parameter to establish the relationships between machining and other parameters with cutting forces for model development.

The assumptions used to simplify the model development are as follows:

1. The diamond abrasive grits/particles are rigid regular octahedron.
2. All the diamond abrasive grits are in the same size.
3. The material removal mode is a rigid brittle fracture.

The following geometric relationship can be obtained from Fig. 1:

$$w = \frac{d}{2\tan\beta} \tag{1}$$

where w is the penetration depth, d is the penetration width, and β is the half angle of an abrasive grit, ($\beta = 45°$). According to the definition of Vickers-hardness, the formula can be obtained as follows:

$$Hv = 0.102 \times \frac{F'_n}{S_{\text{area}}} = 0.102 \times \frac{2F'_n \sin\beta}{d^2} \tag{2}$$

where Hv is the Vickers hardness of workpiece material, F'_n is the axial cutting force of a single diamond abrasive grit on the surface of workpiece material, and S_{area} is the surface area of resulting indentation on workpiece material.

By solving Eq. (1) and Eq. (2) simultaneously, the following relation can be obtained:

$$w = \sqrt{0.051 \cdot \frac{\cos^2\beta}{\sin\beta} \cdot \frac{F'_n}{Hv}} \tag{3}$$

The volume of single diamond grit (v) can be expressed as follows:

$$V = \frac{\sqrt{2}}{3} {S_a}^3 \tag{4}$$

where S_a is the side length of diamond abrasive grit as shown in Fig. 2.

The diamond abrasive concentration is the mass of abrasive per unit volume within working layer. Concentration is generally defined as follows: per cubic centimeter volume of abrasive grains containing 4.4 karats (1 karat diamond is equal to 0.2 g) is defined as 100. Each increasing or decreasing of 1.1 karats of abrasive, then the concentration, is increased or decreased by 25%, respectively. According to this definition, the total number of active diamond abrasive grains involved in cutting, N_α, can be expressed as follows:

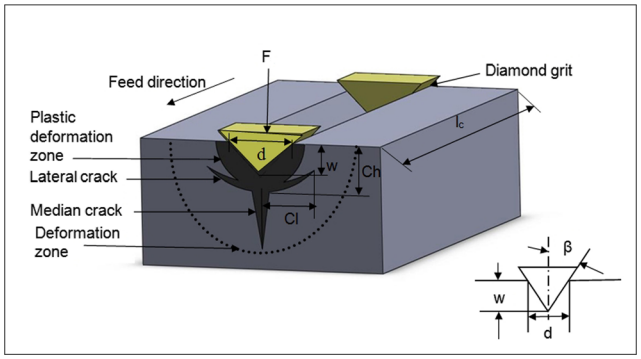

Fig. 1 Crack generation and deformation zone in material

$$N\alpha = \left(\frac{0.88 \times 10^{-3}}{\left(\sqrt{2}/3\right) Sa^3 \cdot \rho} \cdot \frac{C_\alpha}{100} \right)^{2/3} \cdot A_0 = C_1 \cdot \frac{C_\alpha^{\frac{2}{3}}}{Sa^2} \cdot A_0 \tag{5}$$

where ρ is the density of diamond (3.52×10^{-3} g/mm^3), C_α is the diamond abrasive concentration, C_1 is the constant number, $C_1 = 3 \times 10^{-2}$, and A_0 is the area of the cutting tool in contact with the workpiece material (involved in cutting).

2.2 Two cases of face milling

Since the cutting force model is required to be generalized and applicable for the two kinds of tools like cylindrical and conical diamond abrasive core tools, the contact area, A_0, will be different for both kinds of tools and two cases can be found as shown in Fig. 3.

The cutting force F_n (the axial cutting force due to a single diamond grit) and F (the axial cutting force caused by all the active diamond abrasives on the end face of the core tool and measured by dynamometer through experiments) have different angles in case of cylindrical core tool and conical core tool as shown in Fig. 4.

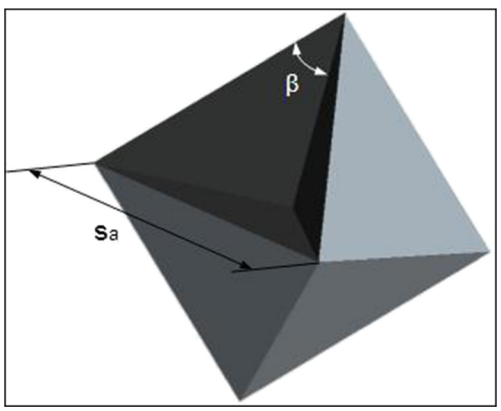

Fig. 2 Octahedron shaped diamond abrasive grit

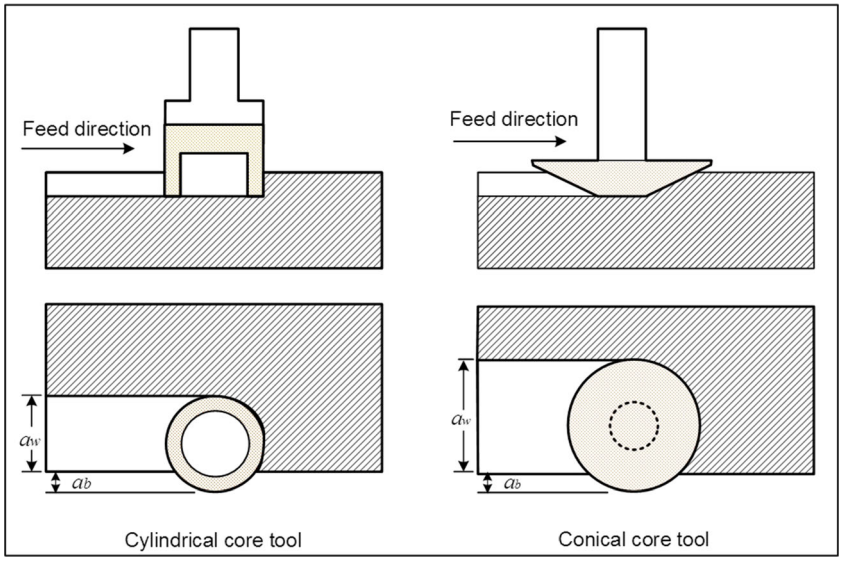

Fig. 3 Face milling with cylindrical and conical abrasive core tool

2.2.1 Face milling with cylindrical abrasive core tool

Figure 3 shows the relationship of the contact area of the face (with workpiece material) and the geometry of both types of abrasive core tools. The contact area, A_0, for cylindrical core tool can be calculated by Eq. (6):

$$A_0 = \pi\left[\left(R_2{}^2 - R_1{}^2\right) + R_2\left(a_p - 2a_b\right) - a_p.a_b\right] \tag{6}$$

where R_1 and R_2 are the inner and outer radii of the diamond core tool, respectively; a_p is the cutting depth; a_w is the cutting width ($a_w = R_2$ for cylindrical core tool); and a_b (in mm) is the overlapping cutting allowance which is the distance of overlap with the machined surface by previous cutting pass of the tool (the distance which is required to leave uncut for smooth cutting surface and to reduce/finish scallop height). Practically, it is required to be considered for accurate face milling. Also, for cylindrical core tool (Fig. 4), the angle between F and F_n is zero (i.e, $\theta = 0°$).

2.2.2 Face milling with conical shaped core tool

The contact area, A_0, for conical core tool can be calculated by Eq. (7).

$$A_0 = \pi R_1^2 + \frac{\pi}{2}\left[\left(2R_1 + a_p\cot\theta - a_b\right)\sqrt{a_p^2(1+\cot^2\theta) + a_b\left(a_b - 2a_p\cot\theta\right)}\right] \tag{7}$$

Also, for cylindrical core tool (Fig. 4), the angle between F and F_n is as under:

$0° < \theta < 90°$.

From Fig. 5, the relation between Z and f can be obtained as follows:

$$Z = A\sin(2\pi ft) \tag{8}$$

where Z is the trajectory of the diamond abrasive grain, A is the amplitude, f is the frequency, and t is the time, respectively.

According to Eq. (8) and Fig. 5, the effective contact time Δt can be expressed as follows:

$$\Delta t = \frac{1}{\pi f}\left[\frac{\pi}{2} - arcsin\left(1 - \frac{w}{A}\right)\right] \tag{9}$$

On the basis of energy conservation theorem, the following relation can be found:

$$I = \int_{\text{cycle}} F_m \cdot dt \approx F_m \cdot \Delta t \tag{10}$$

Also

$$I = \frac{F_n}{f} \tag{11}$$

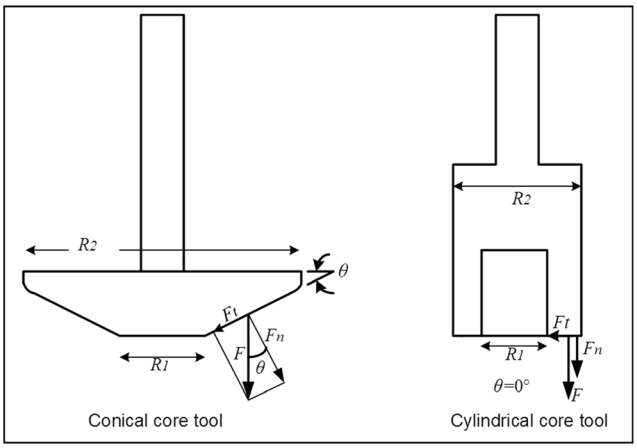

Fig. 4 Relationship of F_n and F for cylindrical and conical core tool

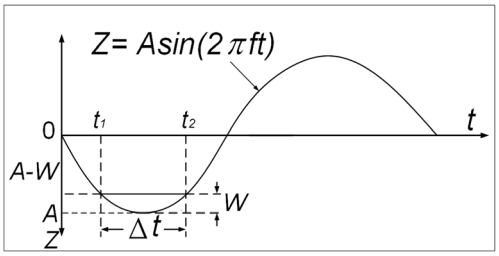

Fig. 5 Relation of effective contact time (Δt) and maximum penetration depth (w)

where I is the impulse, Δt is the effective contact time during which an abrasive grain penetrates into the workpiece, F_m is the axial impact force between core tool and workpiece material, F_n is the axial cutting force, and *cycle* means a vibration cycle of the diamond abrasive grit. From Eq. (10) and Eq. (11), the following relation can be found:

$$F_n = \Delta t \cdot f \cdot F_m \tag{12}$$

The cutting force F_m can also be expressed as follows:

$$F_m = N_\alpha \cdot F_n' \tag{13}$$

Substituting Eq. (9) and Eq. (13) into Eq.(12), then:

$$F_n = \frac{N_\alpha}{\pi}\left[\frac{\pi}{2} - \arcsin\left(1-\frac{w}{A}\right)\right].F_n' \tag{14}$$

From the geometrical relation shown in Fig. 4:

$$F_n = F\cos\theta \tag{15}$$

Then, Eq. (14) can be written as under:

$$F_n = \frac{N_\alpha}{\pi\cos\theta}\left[\frac{\pi}{2} - \arcsin\left(1-\frac{w}{A}\right)\right].F_n' \tag{16}$$

By solving both Eq. (16) and Eq. (3), the relationship between maximum penetration depth and cutting force can be obtained as follows:

$$w = \sqrt{0.051 \cdot \frac{\cos^2\beta}{\sin\beta} \cdot \frac{1}{H_v} \cdot \frac{\pi \cdot F\cos\theta}{N_\alpha \cdot \left[\frac{\pi}{2} - \arcsin\left(1-\frac{w}{A}\right)\right]}} \tag{17}$$

According to the indentation theory and research by Marshall and Lawn [26, 27], the length of lateral crack C_l and the depth/height of lateral crack C_h can be expressed as follows:

$$C_l = C_2 \cdot \left(\frac{1}{\tan\beta}\right)^{5/12} \cdot \left(\frac{E^{3/4}}{H_v K_{IC}(1-\upsilon^2)^{1/2}}\right)^{1/2} \cdot {F_n}^{5/8} \tag{18}$$

$$C_h = C_2 \cdot \left(\frac{1}{\tan\beta}\right)^{1/3} \cdot \frac{E^{1/2}}{H_v} \cdot {F_n}^{1/2} \tag{19}$$

where E is the elastic modulus and ν is the Poisson's ratio of the workpiece material, C_2 is the dimensionless constant number; $C_2 = 0.226$.

The material removal volume as the abrasive grit penetrates into the workpiece has been illustrated in Fig. 6. The penetration depth increases from 0 to w first and then decreases to 0 within period Δt and the side length at C_h is $2C_l$. Accordingly, the theoretical material removal volume V_0 during one penetration period is nearly equal to the volume of the pentahedron $ABCDE$ and can be expressed as follows [28]:

$$L_s = \frac{2\pi SR}{60} \cdot \Delta t \tag{20}$$

$$V_0 = 2V_{\mathrm{ABCD}} = \frac{1}{3} C_l \cdot C_h \cdot L_s \tag{21}$$

where Ls is the length when an abrasive grit of end face of tool moves within one period, Δt R is the distance from the abrasive grit to the center of core tools, and S is the spindle speed. The actual material removal volume (V) within one penetration period is nearly equal to the volume of theoretical material removal volume (V_0). It is assumed that V and V_0 are in linear proportion and can be found as under:

$$V = kV_0 = \frac{1}{3} k \cdot C_l \cdot C_h \cdot \frac{2\pi SR}{60} \cdot \Delta t \tag{22}$$

where k is the constant and that can be obtained mechanistically from cutting force experiments. If MRR_a is the material removal rate of single abrasive grit and V is the material removal volume caused by single abrasive grit in one vibration, then MRR_a can be expressed as follows:

$$MRR_a = f \cdot V = \frac{k.\pi}{90} \cdot C_l \cdot C_h \cdot S \cdot R \cdot \left[\frac{\pi}{2} - \arcsin\left(1-\frac{w}{A}\right)\right] \tag{23}$$

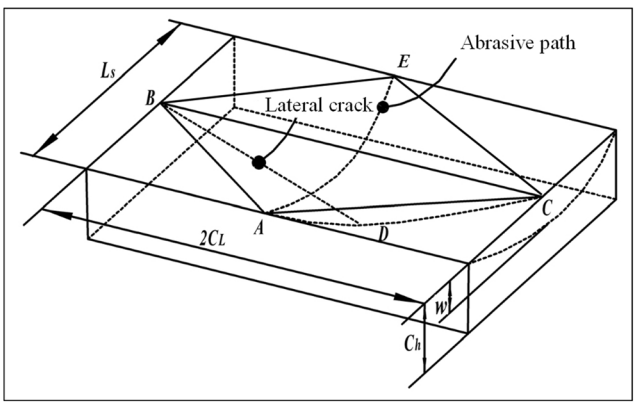

Fig. 6 Illustration for material removal volume calculation

The material removal rate, MRR_T, is the total material removed by all the effective abrasive grits during one period and can be expressed as follows:

$$MRR_T = N_\alpha \cdot MRR_a = N_\alpha \cdot f \cdot V = \frac{k.\pi}{90} \cdot N_\alpha \cdot C_l \cdot C_h \cdot S \cdot R \cdot \left[\frac{\pi}{2} - \arcsin\left(1 - \frac{w}{A}\right)\right] \quad (24)$$

For simplification, the average radius $\left(\frac{R_1+R_2}{2}\right)$ has incorporated instead of R and the contact time Δt (Eq. (9)) can be simplified as follows:

$$\Delta t = \frac{w}{\pi A f} \quad (25)$$

Eq. (25) has been obtained by using the following simplification:

$$\frac{w}{A} \approx \left[\frac{\pi}{2} - \arcsin\left(1 - \frac{w}{A}\right)\right] \quad (26)$$

Eq. (24) can also be written as follows:

$$MRR_T = N_\alpha \cdot MRR_a = N_\alpha \cdot f \cdot V \approx \frac{k.\pi}{90} \cdot N_\alpha \cdot C_l \cdot C_h \cdot S \cdot \frac{R_1 + R_2}{2} \cdot \frac{w}{A} \quad (27)$$

Eq. (17) can be simplified as follows:

$$w = \left(\frac{0.051.\pi.\cos^2\beta.F\cos\theta.A}{\sin\beta.H_v.N_\alpha}\right)^{1/3} \quad (28)$$

By solving Eq. (27) and Eq. (28) with applying $F_m = N_\alpha \cdot F_n^{'}$ (where $F \approx F_m$), the following relation has been obtained:

$$MRR_T = \frac{k.(0.051)^{1/3}.\pi^{1/3}.C_2^2.S.(R_1+R_2).\cos^{2/3}\beta.F^{35/24}.\cos^{35/24}\theta.E^{7/8}.C_1^{2/3}.C_\alpha^{4/9}.A_0^{2/3}}{180.A^{2/3}.\sin^{1/3}\beta.{H_v}^{11/6}.(\tan\beta)^{3/4}.{K_{IC}}^{1/2}.(1-\nu^2)^{1/4}.S_a^{4/3}} \quad (29)$$

The total material removal rate can also be expressed as follows follows:

$$MRR_T = f_r.A_0 \quad (30)$$

where f_r is the feed rate (mm/min) of the abrasive core tool. By solving Eq. (29) and Eq. (30), then relationship of axial cutting force and parameters has been obtained as follows:

$$F = \frac{K}{\cos\theta} \cdot \left[\frac{C_3.\tan^{26}\beta.{K_{IC}}^{12}.{H_v}^{44}.(1-\nu^2)^6.f.A^{16}.S_a^{32}.{f_r}^{24}.A_0^8}{\cos^8\beta.(R_2+R_1)^{24}.E^{21}.S^{24}.C_\alpha^{32/3}}\right]^{1/35} \quad (31)$$

where C_3 is the dimensionless constant number and has value as follows:

$$C_3 = \left[\frac{(180)^{24}}{(0.051)^8.{C_1}^{16}.{C_2}^{48}.\pi^8}\right] \quad (32)$$

Eq. (31) is the desired generalized cutting force prediction model for the axial cutting force, and contact area A_0 can be found from Eq. (6) and Eq. (7) for the cylindrical and the conical abrasive core tool, respectively.

3 Experimental setup and conditions

The schematic and the actual experimental setup have been shown in Fig. 7 and Fig. 8, respectively. The setup is composed of three parts: ultrasonic vibration system, CNC vertical machining center, and diamond core tool. The ultrasonic vibration system has an ultrasonic spindle and an ultrasonic generator. The CNC vertical machining center (Model: VMC 0850B, Shenyang, China) has fitted with ultrasonic vibration device/attachment (developed by Tianjin University, China) having the ultrasonic spindle. The cutting force has been measured with the dynamometer (9257B, Kistler, Switzerland). The main specifications of the machine tool have been mentioned in Table 1. The workpiece material used for experiments is CFRP-T700 having dimensions 96 × 40 × 5 mm and mechanical properties as shown in Table 2. The specifications of the cylindrical and the conical diamond core tool have been mentioned in Table 3. The average grit size 385 μm has been taken here [29]. Also, the value of the amplitude is kept on the higher side (10 μm) and ultrasonic frequency on the lower side (16,000 Hz) for batter results in the case of CFRP material as observed by random experiments. The experimental design has been shown in Table 4.

3.1 Experimental design

On the basis of previous studies and random experiments, the machining parameters like spindle speed, cutting depth, and feed rate have been found significant for cutting forces and have been applied as variables in this research. The experiments have been designed by single factor experiment array with 3 factors. The level of each factor is selected by the theoretical calculations, previous experiments, and keeping in view the higher values of MRR for industrial applications.

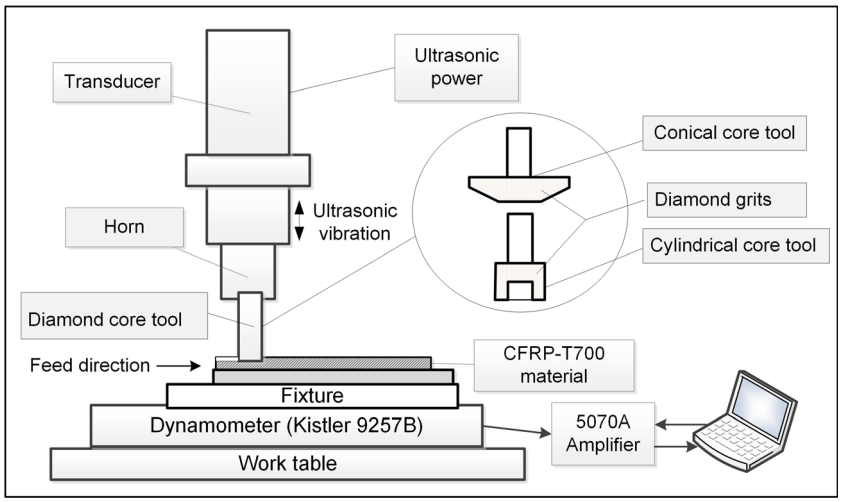

Fig. 7 Schematic diagram of experimental setup

4 Experimental results and discussion

The experiments were conducted corresponding to each group of machining parameters. The machining process has been divided into three stages, i.e., enter, stable, and exit as shown in Fig. 9. The cutting force value is the mean value of maximum values during one period in a stable stage that has been obtained through measurement in graphical form with Dynoware software. The graphical cutting force data then transformed to numerical data through MATLAB software. The axial cutting force data obtained for experiments with the cylindrical core tool has been shown in column 5 of Table 5 and for experiments with the conical core tool has been recorded in column 5 of Table 6, corresponding to each set of their parameters.

4.1 Obtaining of proportionality parameters, K_1 and K_2

It has been found that the simulation values of axial cutting force are closest to measurement values when $\sum(F_{(m)} - K' * F_{(s)})^2$ (where $K = K_1$ for cylindrical core tool and $K = K_2$ for conical core tool) got the minimum value. For this purpose, it is required to differentiate it with respect to K, putting the values for each experiment, sum up the values for all experiments, and then the value of K is obtained. It is the relationship of the workpiece material and properties (geometry, material, etc.) of cutting tool and is not relevant to machining parameters. The value of K_1 and K_2 has been found 0.036 and 0.029, respectively. The cutting force data obtained by applying the cutting force model for cylindrical and conical abrasive core tools have been recorded in Table 5 (column 6) and Table 6 (column6), respectively.

The experimental and simulated data (from the model) of cutting force were then plotted as shown in Fig. 10 and Fig. 11. From the analysis, the simulated values of axial cutting force have been found a close match (nearly equal) with the measured values of cutting forces for cylindrical and conical core tools. Numerically, the measured and simulated values of cutting force have small variation (less than 10%) for cylindrical and conical core tool experiments. However, higher variation (from this value) has been found in Exp. 12 (19.81%) for cylindrical core tool and Exp. 4 (16.42%), Exp. 5 (20.15%), and Exp. 10 (10.73%) for conical core tool. Such variations are mainly due to heterogeneity and anisotropy of CFRP composites. Also, these variations can rise due to uneven material properties and dislocations of fibers. The value of instantaneous cutting force may change more than three times because when machining different cutting area, the

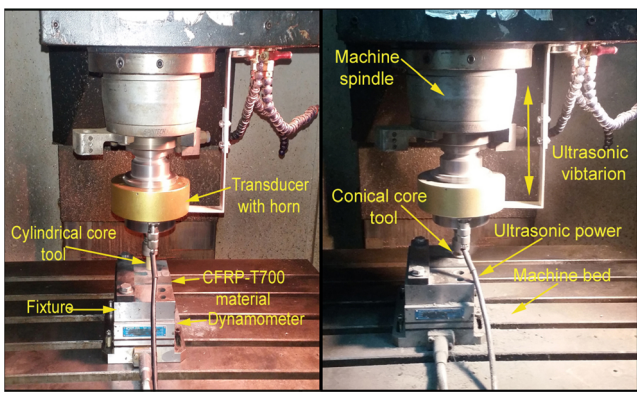

Fig. 8 Actual setup for experiments

Table 1 Properties of machine tool

Nomenclature	Specification
Spindle speed (with ultrasonic device)	0–6000 rpm
Ultrasonic amplitude	10 μm
Ultrasonic frequency	16,000 Hz

Table 2 Mechanical properties of workpiece material

Nomenclature	Specification
Density (ρ)	1.8 g/cm^3
Poisson's ratio (ν)	0.30
Elastic modulus (E)	53GPa
Fracture toughness (K_{IC})	11.5 MPa·m$^{1/2}$
Vickers hardness (Hv)	0.6GPa

average cutting force may change. Other factors contributing to this behavior are their inhomogeneous, and varying thermal behavior. So, the error up to limited level was recorded in some cases. These are expected and required to be accepted due to nature of the material.

The developed cutting force model is applicable for cylindrical as well as conical abrasive core tools by applying the relevant swept/contact area, A_0. Zhang [24] developed the cutting force model for cylindrical core tool whereas Yuan and Zhang [23, 25] have proposed the axial cutting force model for conical core tools. The contact area calculations have improved and the overlapping cutting allowance, a_b, has incorporated to find the results of cutting force model near to practical machining situations in this paper.

The maximum values of feed rate and cutting depth (f_r = 180 mm/min and a_p = 0.8 mm) have been applied to develop the cutting force model whereas the values applied by Zhang [24] are lower at the significant level (f_r = 12 mm/min and a_p = 0.08 mm). The higher values of machining parameters are significant to increase the *MRR* as $MRR = f_r.a_p.a_e$. The cutting force has been found decreased with the increase of spindle speed. The cutting force has been found increased with the increase of feed rate and cutting depth. The same has been also reported by Yuan and Zhang [25].

The generalized model has been developed the first time in this paper and found robust for the both types (cylindrical and conical) of core tools. Also, no research has been reported till yet for rotary ultrasonic face milling of CFRP, especially for CFRP-T700 composites. However, the cutting force models have developed for RUFM of K9 optical glass and C/Sic materials [24, 25].

Table 3 Properties of diamond abrasive core tool

Nomenclature	Specification	
Tool type	Cylindrical	Conical
Abrasive	Diamond	Diamond
Bond type	Metal-bond	Metal-bond
Mesh size	40/45	40/45
Concentration (C_α)	100	100
Outer radius (R_2)	6.25 mm	13 mm
Inner radius (R_1)	4.75 mm	4.75 mm
Angle (θ)	0°	15°

Table 4 Experimental design

Group	Experiments	Spindle speed, S (rpm)	Feed rate, f_r (mm/min)	Cutting depth, a_p (mm)
1	1–6	2000, 2500, 3000, 3500, 4000, 4500	60	0.5
2	7–11	3000	60, 90, 120, 150, 180	0.5
3	12–15	3000	60	0.5, 0.6, 0.7, 0.8

4.2 Validation of cutting force model

The additional experiments were carried out to find that the variation/error is random or due to some issues in the cutting force model. The related data has been reported in Table 7 and Table 8 and has been plotted as shown in Fig. 12 and Fig. 13. The experiments have designed on the basis of full factorial design with 2-level of parameters (S, f_r, and a_p) for cylindrical and conical core tools using Minitab 16 software. From graphical plots, it has been found that the most of the data points are closely matched for measured and simulated values of cutting force for both types of the tools. The variation more than 10% has been found in two experiments (Exp. 1 as 23.20% and Exp. 5 as 16.90%) for cylindrical core tool whereas two experiments (Exp. 2 as 13.88% and Exp. 7 as 20.47%). These variations show the similar behavior of higher variation for CFRP composites and supported the findings that higher variations in cutting forces may sometimes occur due to inhomogeneity, heterogeneity, anisotropy, and some other factors as mentioned in discussion.

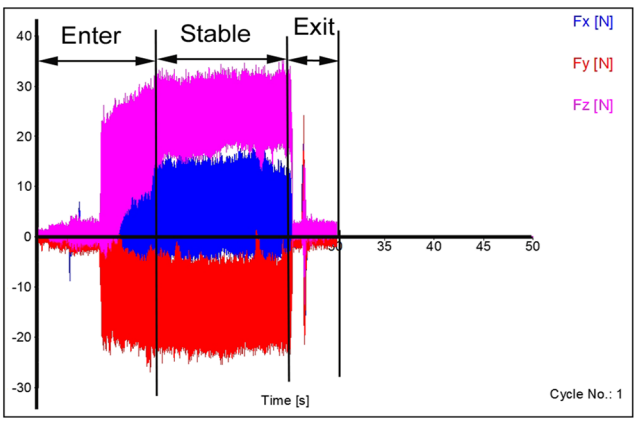

Fig. 9 Cutting force measurements (Exp. No. 3 of Table 5 with S = 3000 rpm, f_r = 60 mm/min, a_p = 0.5 mm, cylindrical core tool)

Table 5 Measured and simulated axial cutting force data for cylindrical core tool

Exp. No	*S (rev/min)*	f_r *(mm/min)*	a_p *(mm)*	Measured axial force $(F_{(m)})$ *(newton)*	Simulated axial force $(F_{(s)}$ *without* $K_1)$ *(newton)*	Simulated axial force $(F'_{(s)}$ *with* $K_1)$ *(newton)*	Error $\frac{\left(F'_{(s)}-F_{(m)}\right)}{F_{(m)}} \times 100\%$
1	2000	60	0.5	16.921	453.232	16.316	−3.57
2	2500	60	0.5	14.980	388.927	14.001	−6.53
3	3000	60	0.5	13.104	343.220	12.355	−5.71
4	3500	60	0.5	10.677	308.792	11.116	+4.11
5	4000	60	0.5	9.892	281.773	10.143	+2.53
6	4500	60	0.5	9.215	259.911	9.356	+1.53
7	3000	60	0.5	12.404	343.220	12.355	−0.39
8	3000	90	0.5	15.845	453.232	16.316	+2.97
9	3000	120	0.5	20.842	552.069	19.874	−4.64
10	3000	150	0.5	22.080	643.348	23.160	+4.89
11	3000	180	0.5	25.918	729.024	26.244	+1.25
12	3000	60	0.5	10.312	343.220	12.355	+19.81
13	3000	60	0.6	12.312	345.688	12.444	−2.97
14	3000	60	0.7	13.309	348.098	12.531	−5.84
15	3000	60	0.8	13.875	350.454	12.616	−9.07

5 Conclusions

From the presented research work, the conclusions that have been drawn are as follows:

1. The generalized cutting force prediction model has been developed for RUFM of CFRP-T700 composites with cylindrical and conical abrasive core tools. The measured and the simulated values of cutting forces found closely matched. However, the variation higher than10% has been also observed in the few groups of experiments. This variation is due to the inhomogeneity, heterogeneity, anisotropy, and some other properties of such materials. So, the developed cutting force model is accurate/robust and can be applied for finding cutting forces.

Table 6 Measured and simulated axial cutting force data for conical core tool

Exp. No	*S (rev/min)*	f_r *(mm/min)*	a_p *(mm)*	Measured axial force $(F_{(m)})$ *(newton)*	Simulated axial force $(F_{(s)}$ *without* $K_1)$ *(newton)*	Simulated axial force $(F'_{(s)}$ *with* $K_1)$ *(newton)*	Error $\frac{\left(F'_{(s)}-F_{(m)}\right)}{F_{(m)}} \times 100\%$
1	2000	60	0.5	11.481	375.422	10.887	−5.17
2	2500	60	0.5	9.750	322.157	9.340	−4.18
3	3000	60	0.5	9.012	284.297	8.244	−8.52
4	3500	60	0.5	8.875	255.779	7.417	−16.42
5	4000	60	0.5	5.439	233.399	6.768	+20.15
6	4500	60	0.5	5.724	215.290	6.243	+9.06
7	3000	60	0.5	8.125	284.297	8.244	−2.03
8	3000	90	0.5	10.070	375.422	10.887	+8.11
9	3000	120	0.5	12.617	457.291	13.261	+5.10
10	3000	150	0.5	13.956	532.899	15.454	+10.73
11	3000	180	0.5	16.060	603.866	17.512	+9.04
12	3000	60	0.5	8.097	284.297	8.244	+1.81
13	3000	60	0.6	8.623	289.917	8.407	−2.50
14	3000	60	0.7	9.140	295.472	8.568	−6.25
15	3000	60	0.8	9.758	300.960	8.727	−3.65

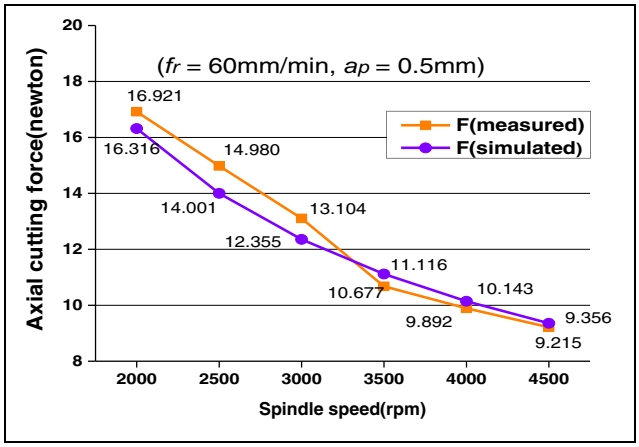

(a)

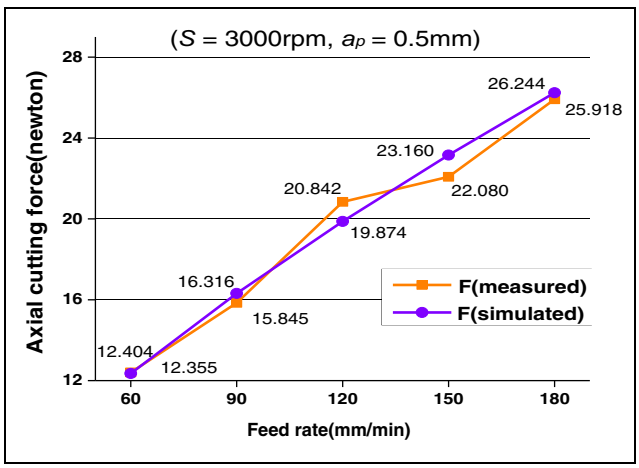

(b)

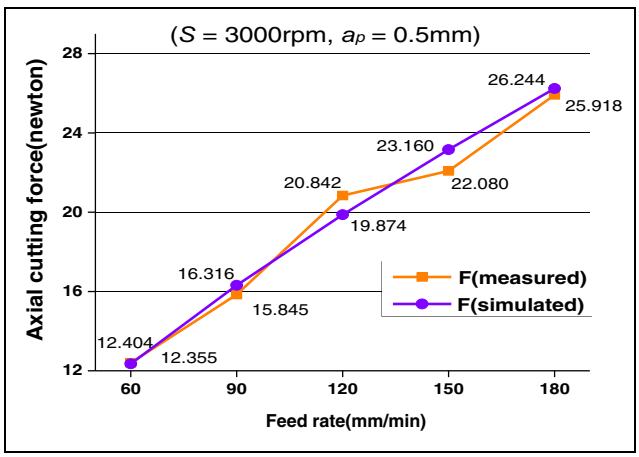

(c)

Fig. 10 Relationship of cutting force and machining parameters for cylindrical core tool

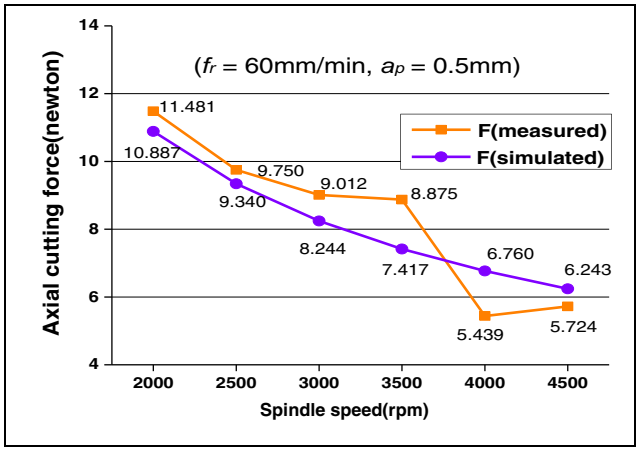

(a)

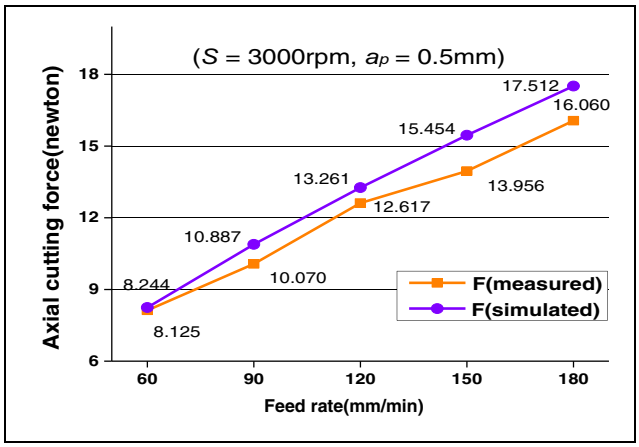

(b)

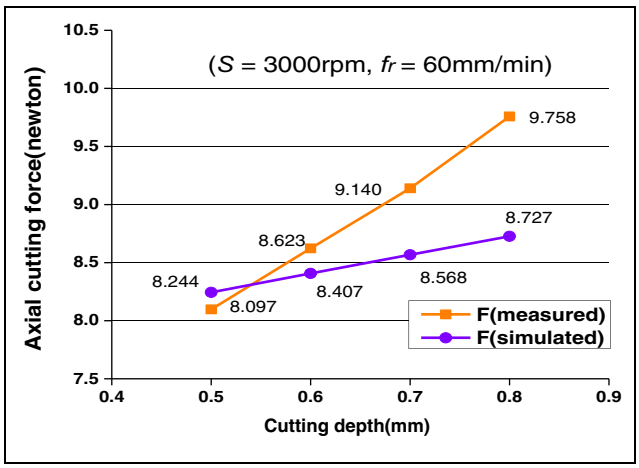

(c)

Fig. 11 Relationship of cutting force and machining parameters for conical core tool

2. The developed cutting force model is the generalized model which is applicable to diamond abrasive core tools having the range of angle, θ, as follows: $0^{\circ} \leq \theta < 90^{\circ}$ (Fig. 4).

3. The model is applicable for cylindrical and conical core tools using the relevant contact area, A_0. The improved formulae for A_0 have been proposed and the overlapping

Table 7 Measured and simulated axial cutting force data for cylindrical core tool

Exp. No	*S (rev/min)*	f_r *(mm/min)*	a_p *(mm)*	Measured axial force $(F_{(m)})$ *(newton)*	Simulated axial force $(F_{(s)}$ *without* $K_1)$ *(newton)*	Simulated axial force $(F'_{(s)}$ *with* $K_1)$ *(newton)*	Error $\frac{\left(F'_{(s)}-F_{(m)}\right)}{F_{(m)}} \times 100\%$
1	5000	100	1.2	10.500	359.377	12.937	+23.20
2	3500	100	0.6	15.188	441.472	15.892	+4.63
3	5000	200	1.2	22.015	578.057	20.810	−5.47
4	5000	200	0.6	19.887	556.039	20.017	+0.65
5	3500	100	1.2	14.133	458.953	16.522	+16.90
6	3500	200	0.6	24.875	710.107	25.560	+2.75
7	3500	200	1.2	27.213	738.226	26.576	−2.34
8	5000	100	0.6	12.960	345.688	12.444	−4.00

Table 8 Measured and simulated axial cutting force data for conical core tool

Exp. No	*S (rev/min)*	f_r *(mm/min)*	a_p *(mm)*	Measured axial force $(F_{(m)})$ *(newton)*	Simulated axial force $(F_{(s)}$ *without* $K_1)$ *(newton)*	Simulated axial force $(F'_{(s)}$ *with* $K_1)$ *(newton)*	Error $\frac{\left(F'_{(s)}-F_{(m)}\right)}{F_{(m)}} \times 100\%$
1	5000	100	1.2	10.062	322.200	9.343	−7.14
2	3500	100	0.6	9.428	370.248	10.737	+13.88
3	5000	200	1.2	16.013	518.258	15.029	−6.14
4	5000	200	0.6	12.573	466.331	13.523	+7.55
5	3500	100	1.2	12.697	411.476	11.932	−6.02
6	3500	200	0.6	16.680	595.543	17.270	+3.53
7	3500	200	1.2	24.134	661.858	19.193	−20.47
8	5000	100	0.6	8.241	289.917	8.407	+2.01

cutting allowance, a_b, has been incorporated for accurate machining.

4. The significantly higher values of machining parameters have been applied (f_r = 200 mm/min a_p = 1.2 mm, S = 5000 rpm) for the first time for higher MRR and practical machining conditions. The cutting force has been found decreased with the increase of spindle speed; however, it has been found increased with the increase of feed rate and cutting depth.

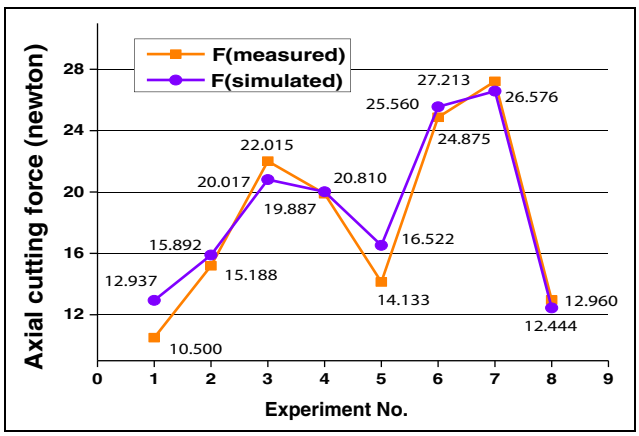

Fig. 12 Cutting force for experiments with cylindrical core tool

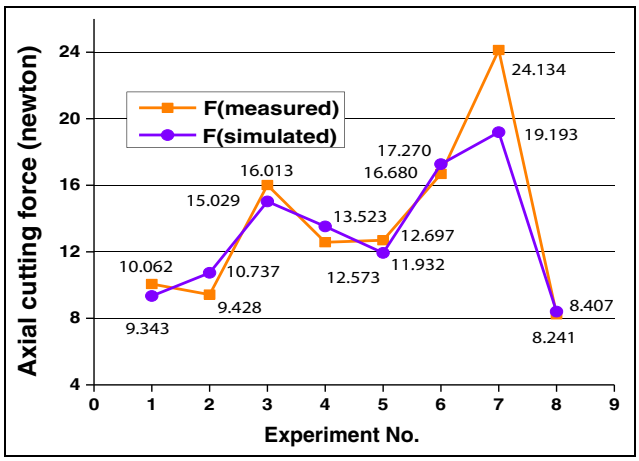

Fig. 13 Cutting force for experiments with conical core tool

The developed generalized cutting force model in this paper can be applied for prediction/minimizing of cutting forces, the increase of product quality, and optimizing the process for rotary ultrasonic face milling of CFRP composites in the industry.

Acknowledgements This research is financially supported by National High Technology Research and Development Program of China under program No. 863 with Grant No. 2013AA040105. The authors are indebted to this financial support to accomplish this research.

References

1. Jones RM (1999) Mechanics of composite materials, 2nd edn. Tylor & Francis Inc., Philadelphia
2. Kaw AK (2006) Mechanics of composite materials, 2nd edn. Taylor & Francis Group, United Kingdom
3. Saoubi RM, Axinte D, Soo LS, Nobel C, Attia H, Kappmeyer G, Engin S, Sim W (2015) High performance cutting of advanced aerospace alloys and composite materials. CIRP Ann Manuf Technol 64:577–580
4. Sheikh-Ahmad JY (2009) Machining of polymer composites. Springer Sci, New York. doi:10.1007/978-0-387-68619-6
5. Liu DF, Tang YJ, Cong W (2012) A review of mechanical drilling for composite laminates. Compos Struct 94:1265–1279
6. Kalla D, Sheikh-Ahmad JY, Twomey J (2010) Prediction of cutting forces in helical end milling of fiber reinforced polymers. Int J Mach Tools Manuf 50:882–891
7. Chen ST, Jiang ZH, Wu YY, Yang HY (2011) Development of a grinding–drilling technique for holing optical grade glass. Int J Mach Tools Manuf 51(2):95–103
8. Groover MP (2010) Fandamental of modern manufacturing: materials, processes, and systems, 4th edn. John wiley & Sons. Inc, Hoboken
9. Yuan S, Zhang C, Amin M, Fan H, Liu M (2015) Development of a cutting force prediction model based on brittle fracture for carbon fiber reinforced polymers for rotary ultrasonic drilling. Int J Adv Manuf Technol. doi:10.1007/s00170-015-7269-x
10. Xu W, Zhang LC, Wu Y (2014) Elliptic vibration-assisted cutting of fibre-reinforced polymer composites: understanding the material removal mechanisms. J comp sci technol 92:103–111
11. Pei ZJ, Prabhakar D, Ferreira PM, Haselkorn M (1995) A mechanistic approach to the prediction of material removal rates in rotary ultrasonic machining. J Eng Ind 117(2):142–151
12. Lau WS, Wang M, Lee WB (1990) Electric discharge machining of carbon fibre composite materials. Int J Mach Tools Manuf 30(2): 297–308
13. Alberadi A, Artaza T, Suarez A, Rivero A, Girot F (2016) An experimental study on abrasive water jet cutting on CFRP/TiA14V stacks for drilling operations. Int J Adv Manuf Technol 86:691–704. doi:10.1007/s00170-015-8192-x
14. Yuan S, Fan H, Amin M, Zhang C, Guo M (2016) A cutting force prediction dynamic model for side milling of ceramic matrix composites C/SiC based on rotary ultrasonic machining. Int J Adv Manuf Technol 86:37–48. doi:10.1007/s00170-015-8099-6
15. Ladonne M, Cherif M, Landon Y, Navez JK, Cahuc O, Castelbajac CD (2015) Modelling the vibration-ssisted drilling process: identification of influential phenomena. Int J Adv Manuf Technol 81: 1657–1666
16. Li ZC, Jiao Y, Deines TW, Pei ZJ, Treadwell C (2005) Rotary ultrasonic machining of ceramic matrix composites: feasibility study and designed experiments. Int J Mach Tools Manuf 45: 1402–1411
17. Gong H, Fang FZ, XTH X (2010) Kinematic view of tool life in rotary ultrasonic side milling of hard and brittle materials. Int J Mach Tools Manuf 50(3):303–307
18. Liu J, Zhang D, Qin L, Yan L (2012) Feasibility study of the rotary ultrasonic elliptical machining of carbon fiber reinforced plastics (CFRP). Int J Mach Tools Manuf 53:141–150
19. Geng D, Zhang D, Xu Y, He F, Liu D, Duan Z (2015) Rotary ultrasonic elliptical machining for side milling of CFRP: tool performance and surface integrity. Ultrasonics 4(3):157–162 **59:128-137**
20. Pei ZJ, Ferreira PM, Haselkorn M (1994) Rotary ultrasonic drilling and milling of ceramics. Paper presented at the Design for Manufacturability and Manufacture of Ceramic Components Symposium, 96 th Ann meet, Am Ceram Soc
21. Pei ZJ, Ferreira PM (1999) An experimental investigation of rotary ultrasonic face milling. Int J Mach Tools Manuf 39:1327–1344
22. Feng DJ, Zhao FL, Xu ZG, Guo DM (2006) Mathematic model of material removal rate for ultrasonic milling. China J Mech Eng 17(13):1399–1403
23. Yuan S, Zhang C, Hu J (2014) Effects of cutting parameters on ductile material removal mode percentage in rotary ultrasonic face machining. Proc Inst Mech Eng B J Eng Manuf 229(9):1547–1556
24. Zhang CL, Zhang JF, Feng PF (2013) Mathematical model for cutting force in rotary ultrasonic face milling of brittle materials. Int J Adv Manuf Technol 69(1–4):161–170. doi:10.1007/s00170-013-5004-z
25. Zhang C, Yuan S, Amin M, Fan H, Liu Q (2015) Development of a cutting force prediction model based on brittle fracture for C/SiC in rotary ultrasonic face milling. Int J Adv Manuf Technol. doi:10.1007/s00170-015-7894-x
26. Marshall DB, Lawn BR, Evans AG (1982) Elastic/plastic indentation damage in ceramics: the lateral crack system. J Am Ceram Soc 65(11):561–566
27. Lawn BR, Evans AG, Marshall DB (1980) Elastic/plastic indentation damage in ceramics: the median/radial crack system. J Am Ceram Soc 63(9–10):574–581
28. Collins JA (1981) Failure of materials in mechanical design. Wiley, New York
29. www. inlandcraft.com/uguides/lapidary_grit_chart.pdf. Accessed 15 September 2016